Supporting Information For

Experimental identification of critical condition for drastically enhancing thermoelectric power factor of two-dimensional layered materials

Junwen Zeng,[†,⊥,#] Xin He,[‡,#] Shi-Jun Liang,[*,†,#] Erfu Liu,[†] Yuanhui Sun,[‡] Chen Pan,[†] Yu Wang,[†] Tianjun Cao,[†] Xiaowei Liu,[†] Chengyu Wang,[†] Lili Zhang,[†] Shengnan Yan,[†] Guangxu Su,[†] Zhenlin Wang,[†] Kenji Watanabe,[§] Takashi Taniguchi,[§] David J. Singh[∥,‡], Lijun Zhang[*,‡] and Feng Miao[*,†]

[†] National Laboratory of Solid State Microstructures, School of Physics, Collaborative Innovation Center of Advanced Microstructures, Nanjing University, Nanjing 210093, China

[‡] Key Laboratory of Automobile Materials of MOE, State Key Laboratory of Superhard Materials, and School of Materials Science, Jilin University, Changchun 130012, China

[§] National Institute for Materials Science, 1-1 Namiki Tsukuba, Ibaraki 305-0044, Japan

[∥] Department of Physics and Astronomy, University of Missouri, Columbia, MO 65211-7010 USA

[⊥] Center for Excellence in Superconducting Electronics, State Key Laboratory of Functional Material for Informatics, Shanghai Institute of Microsystem and Information Technology, Chinese Academy of Sciences, Shanghai 200050, China

[#] These authors contributed equally to this work.

[*] E-mail: miao@nju.edu.cn (F.M.).

[*] E-mail: lijun_zhang@jlu.edu.cn (L.Z.).

[*] E-mail: sjliang@nju.edu.cn (S.J.L.).

V. The measured mobility in the samples with different thickness

VI. Normalization of the power factor with the value of 29 nm

VII. Calculated PF as a function of carrier density in much thinner InSe samples

I. Seebeck coefficient measurement

We used the source and drain electrodes as micro-thermometers to measure the local temperatures. Four-terminal method has been used to measure two micro-thermometers resistance R_{th1} and R_{th2} as a function of the cryostat temperature $T_{cryostat}$ to calibrate the relation between R_{th} and $T_{cryostat}$ (Figure S1a). Applying a voltage V_{heat} to the micro-heater will generate Joule heat with power of V_{heat}^2/R_{heat}, with R_{heat} being the resistance of micro-heater, as a result, local temperature (T_{th1}, T_{th2}) and the corresponding resistance of source and drain electrodes will be increased (Figure S1b). With the relation between R_{th} and $T_{cryostat}$, the increase of temperature for each electrode (dT_{th1}, dT_{th2}) can be calculated. As shown in Figure S1c, we obtained the temperature gradient dT along conducting InSe channel based on the difference between dT_{th1} and dT_{th2}. Meanwhile, we also measured the temperature gradient generated thermoelectric voltage (dV), as shown in the inset of Figure S1c. With the information obtained above, dV as a function dT (see Figure S1d), shows a liner dependence. Thus, we can obtain Seebeck coefficient by $S = -dV/dT$.

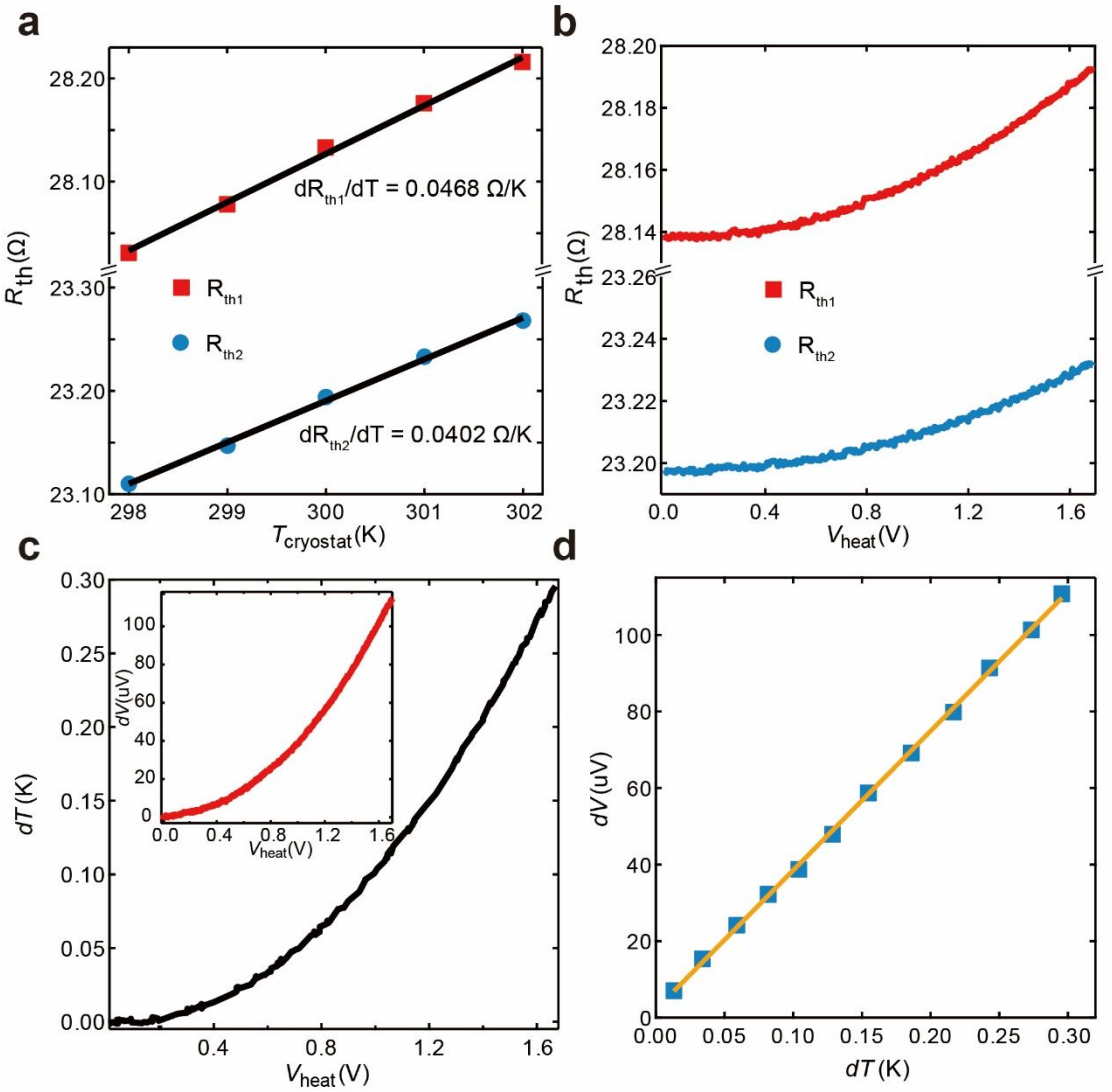

Figure S1. Thermoelectric Seebeck coefficient measurement. (a) Calibration of the relation between the micro-thermometers resistance R_{th1}, R_{th2} and cryostat temperature. Both of R_{th1} and R_{th2} shows a liner dependence of $T_{cryostat}$. The slope is calculated to be 0.0468 Ω/K and 0.0402 Ω/K for $R_{th1}(T_{cryostat})$ and $R_{th2}(T_{cryostat})$, respectively. (b) Micro-thermometers resistance as a function of V_{heat}. Both of R_{th1} and R_{th2} is proportion to V_{heat}^2. (c) Temperature gradient dT vs V_{heat}. Inset is the corresponding thermoelectric voltage dV vs V_{heat}. (d) Thermoelectric voltage dV vs temperature gradient dT shows a linear dependence.

II. Comparison between measured *S* and Mott relation

The Mott relation (described below) describing the temperature and carrier density-

dependent S behavior [1,2] is given by.

$$S = -\frac{\pi^2 k_B^2 T d\ln(\sigma_{2D})}{3e \quad dE}\Big|_{E=E_F} = -\frac{\pi^2 k_B^2 T}{3e}\frac{d\sigma_{2D}}{\sigma_{2D}}\frac{dV_{bg}}{dV_{bg}}\frac{dV_{bg}}{dE}\Big|_{E=E_F}, \qquad (1)$$

where, e, k_B, E, E_F, σ_{2D}, V_{bg} is the elementary charge, Boltzmann constant, energy of charge carrier, Fermi energy, conductivity and gate voltage, respectively. For simplicity, we here consider a parabolic band dispersion. The final expression relies on the approximation that change of Fermi level with gating is the same as the energy dependence without gating, i.e. that the change in carrier density with gating does not affect the electronic properties, i.e. band structure and scattering. With spin degenerate of $g = 2$, and carrier density $n = (V_{bg} - V_{th}) \times C_g$ (where C_g, V_{th} is the capacitance per unit area between sample and back gate threshold voltage respectively), we achieve $\frac{dV_{bg}}{dE} = \frac{em^*}{C_g \pi \hbar^2}$. Thus, the Mott formula for a parabolic band (Eq. (1)) can be written as

$$S = -\frac{2\pi m^* k_B^2 T}{3C_g \hbar^2}\frac{d\sigma_{2D}}{\sigma_{2D} dV_{bg}}, \qquad (2)$$

Based on Eq. (2), we can obtain the carrier density dependence of Seebeck coefficient S_{MR}. In Figure S2, we compared the theory (based on Eq. (2)) to our measured data, and we find that they show a large discrepancy, which may be due to the simplified energy dispersion or dependence of density of states.

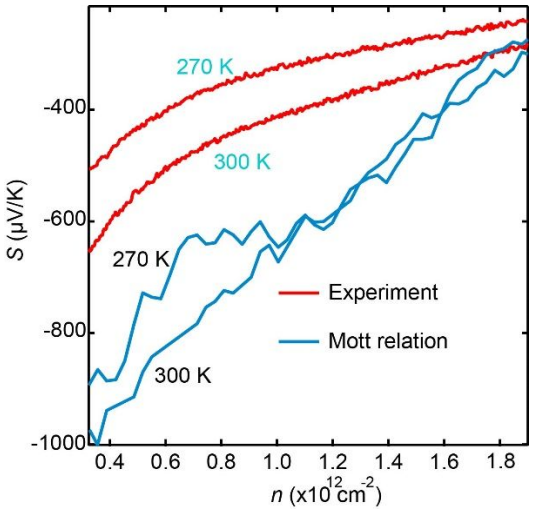

Figure S2. Comparison of Seebeck coefficient determined by Mott relation with experimental data measured in a typical 10 nm thick InSe sample. Two red lines represent measured S at T = 270 K and 300 K, respectively. The blue lines correspond to theoretical results based on Eq. (2).

III. Band structure and DOS of InSe with different thickness

With the ab initio calculations method shown in the main text, we obtained the thickness dependence of electronic band structures and DOS, with results shown in Figure S3. Similar to semiconducting transition metal dichalcogenides, the band gap increases as the thickness is reduced. The reduced thickness leads to stronger quantum confinement, making the DOS of InSe much sharper features. In table S1, we summarized the calculated band gap, effective mass and thermal de Broglie wavelength for different-thickness InSe samples. The calculated band structures and DOS, together with the Boltzmann transport theory were used for calculating the Seebeck coefficient (as seen in the Figure 2c and Figure 3a in the main text). With the thickness-dependent effective mass, the thickness dependence of thermal de Broglie wavelength can be determined, as shown in the Figure 5 in the main text.

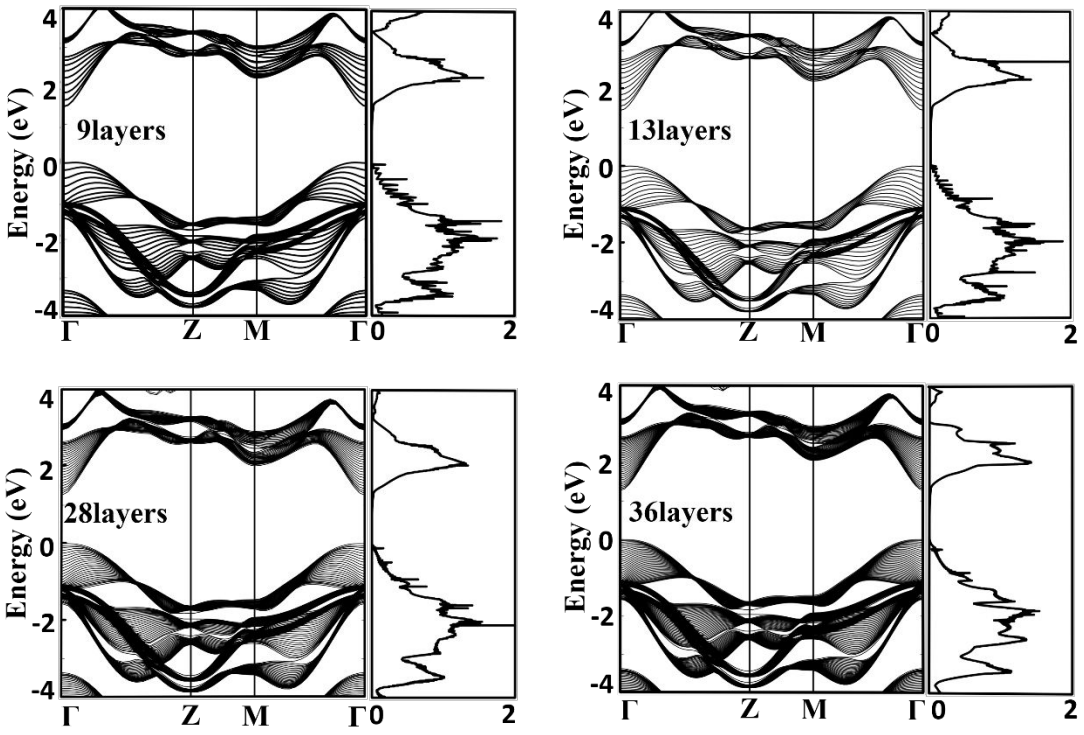

Figure S3 Thickness dependence of band structure and DOS.

Table S1. Summary of thickness dependence of the band gap, effective mass and thermal de Broglie wavelength for InSe samples.

Sample thickness	7nm	10nm	22nm	29nm	Bulk
Number of structure layer	9L	13L	28L	36L	Bulk
Band gap (eV)	1.43	1.42	1.36	1.34	1.315
Effective mass (m_0)	0.153	0.149	0.146	0.145	0.138
Thermal de Broglie wavelength (nm)	11.00	11.14	11.22	11.27	11.55

IV. Conductivity (σ_{3D}) of InSe with different thickness

To obtain the power factor of InSe with different thickness, measurement of the electrical conductivity of InSe are required. With the four terminal method, we show the σ_{3D} as a function of carrier density n in Figure S4.

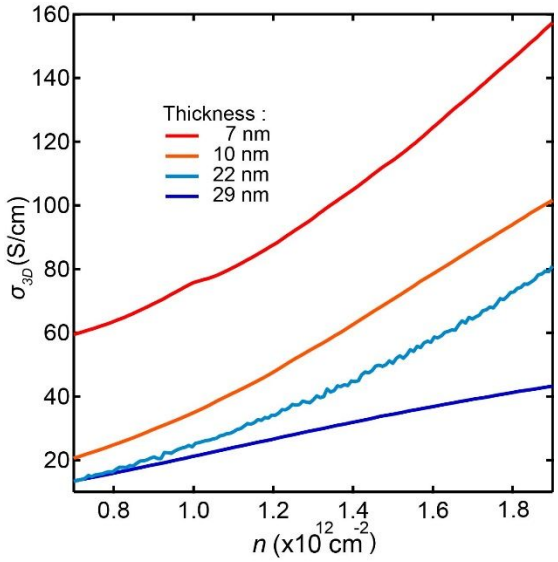

Figure S4 σ_{3D} of InSe with different thickness (7 - 29 nm). $\sigma_{3D} = \sigma_{2D}/h_0$, with h_0 being the thickness of sample.

V. The measured mobility in the samples with different thickness

To analyze the influence of mobility on the thermoelectric power factor, we summarized the mobilities of all the measured devices as a function of thickness at n

=1.9×10^{12} cm^{-2} in Figure S5. We can see the mobility aviaries with thickness, however, there is no obvious dependency between them. In spite of irregular variation of mobility with the thickness, the conclusion in the main text remains unchanged that power factor will be enhanced in the thin samples.

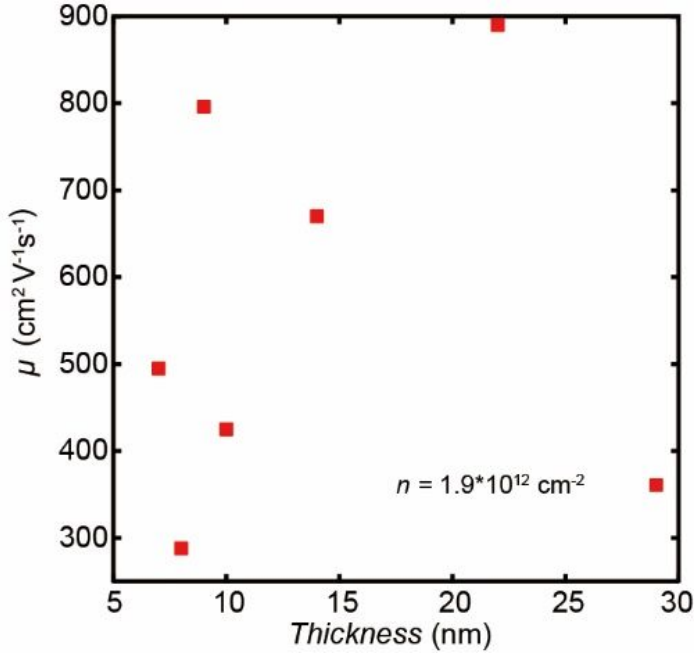

Figure S5 Mobility as a function of thickness.

VI. Normalization of the power factor with the value of 29 nm

For a clear view of the enhancement with decreasing the ratio of quantum confinement length L ($L \approx h_0$, h_0 is the thickness of device) and thermal de Broglie wavelength ξ, we normalized the thickness dependent power factor with the value of 29 nm at three fixed carrier densities. We find that the PF increases with decreasing the h_0/ξ, especially for the regime of $h_0/\xi \leqslant 1$.

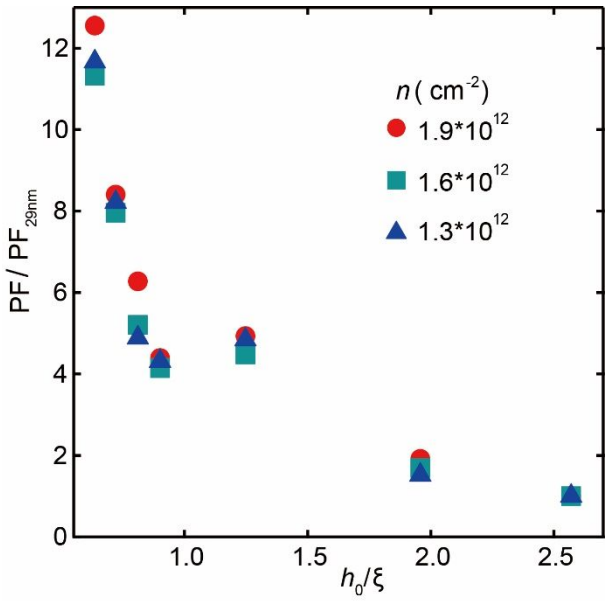

Figure S6 PF/PF$_{29nm}$ as a function of h_0/ξ.

VII. Calculated PF as a function of carrier density in much thinner InSe samples

To further investigate how the intrinsic thermoelectric power factor performance evolves in thinner samples (< 7 nm), we carried out the first-principle calculations for the PF of 1L, 3L, 5L, 9L, 36L as a function of carrier density at T =300 K in the clean limit. The PF calculations were performed based on the Boltztrap code with a constant relaxation time τ of 4.5×10^{-14} s, estimated from $\tau = \frac{\bar{\mu} m_e^*}{e}$, $\bar{\mu}$ is the averaged mobility. We observe that PF is continuously enhanced by thickness reduction down to the monolayer. The results are consistent with the main conclusion in the main text.

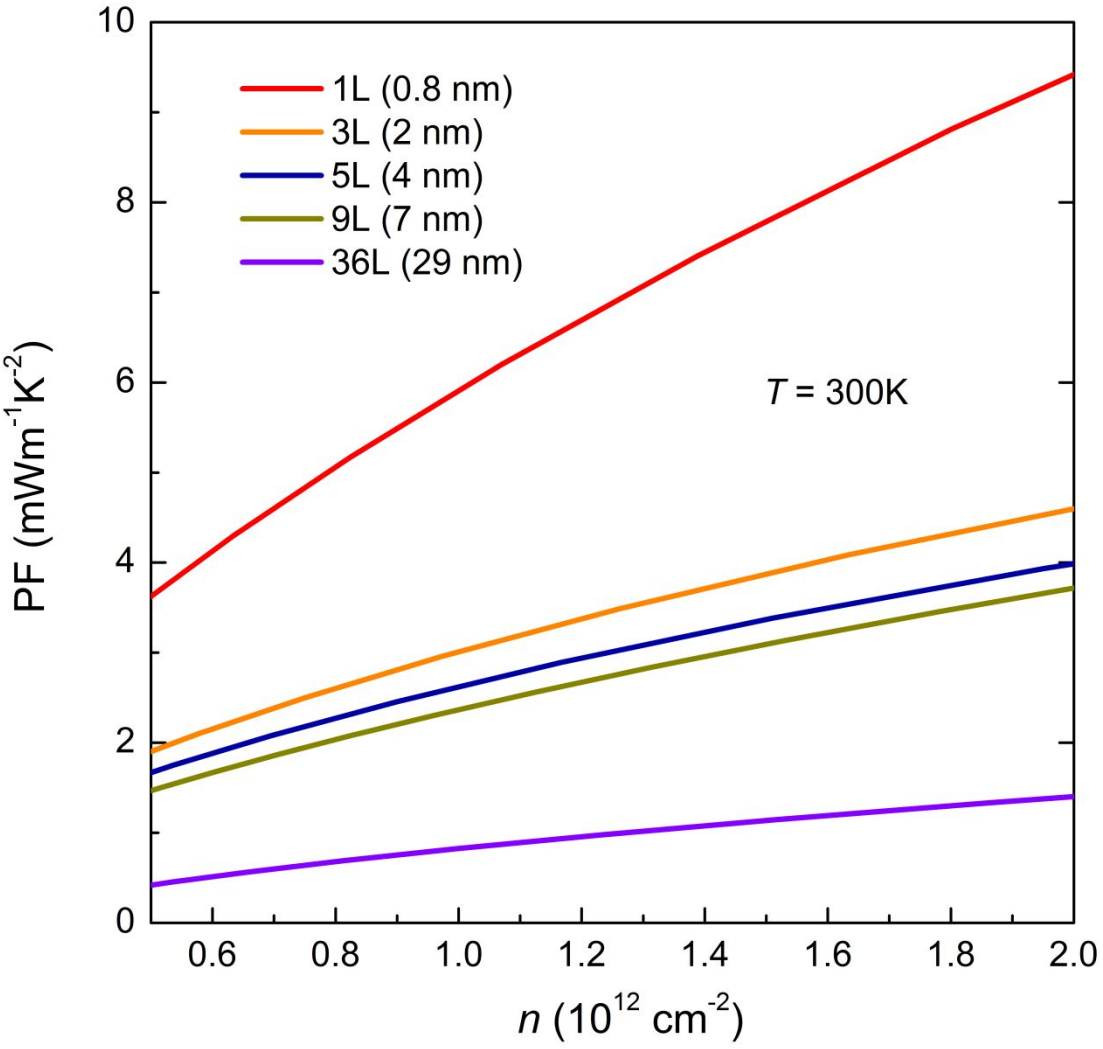

Figure S7 PF vs *n* of 1L, 3L, 5L, 9L, 36L at *T* = 300 K.

REFERENCES

(1) Zuev, Y. M.; Chang, W.; Kim, P. *Phys. Rev. Lett.* **2009**, 102, 96807.

(2) Cutler, M.; Mott, N. F. *Phys. Rev.* **1969**, 181, 1336-1340.